JACS
JOURNAL OF THE AMERICAN CHEMICAL SOCIETY

ARTICLE

pubs.acs.org/JACS

DNA Nanostructures as Models for Evaluating the Role of Enthalpy and Entropy in Polyvalent Binding

Jeanette Nangreave, Hao Yan, and Yan Liu*

Department of Chemistry and Biochemistry and Biodesign Institute, Arizona State University, Tempe, Arizona 85287, United States

Supporting Information

ABSTRACT: DNA nanotechnology allows the design and construction of nanoscale objects that have finely tuned dimensions, orientation, and structure with remarkable ease and convenience. Synthetic DNA nanostructures can be precisely engineered to model a variety of molecules and systems, providing the opportunity to probe very subtle biophysical phenomena. In this study, several such synthetic DNA nanostructures were designed to serve as models to study the binding behavior of polyvalent molecules and gain insight into how small changes to the ligand/receptor scaffolds, intended to vary their conformational flexibility, will affect their association equilibrium. This approach has yielded a quantitative identification of the roles of enthalpy and entropy in the affinity of polyvalent DNA nanostructure interactions, which exhibit an intriguing compensating effect.

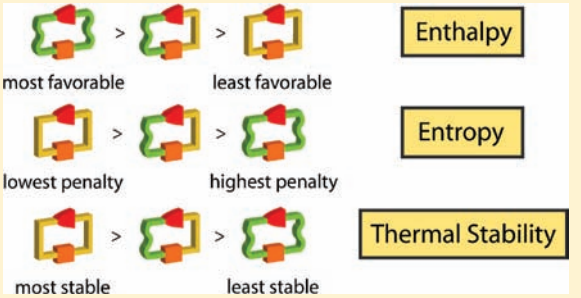

INTRODUCTION

Polyvalent interactions are essential to the function of many biological systems. They are characterized by the simultaneous, specific association of multiple ligands on one molecule to complementary receptors on another molecule and may have unique collective properties as compared to the corresponding monovalent interactions.[1] In medicinal chemistry there is a need to design more effective (efficient) polyvalent inhibitor or promoter drugs, which requires a clear and comprehensive understanding of the thermodynamics of the reaction between inhibitor and target molecules. The collection of ligands in a synthetic, polyvalent molecule can be covalently or non-covalently linked to a backbone molecule, commonly referred to as a scaffold, whose conformational flexibility has a considerable effect on the affinity for a target. Notably, scaffold flexibility can affect both the entropic and enthalpic aspects of binding. To better understand these effects, a polyvalent scaffold with tunable conformational flexibility is required.

DNA nanotechnology offers a unique opportunity to probe the thermodynamics of polyvalent interactions; synthetic DNA nanostructures can be used to gain insight about how subtle changes to ligand/receptor scaffolds may affect their association. DNA nanostructures have previously been used as models to demonstrate that both the number of linkers between scaffolds and their spatial arrangement have significant effects on the stability and thermodynamics of intermolecular binding.[2] The basic building blocks of DNA nanostructures are referred to as "tiles", which are collections of double-helical DNA domains connected by periodic crossovers. Complementary, single-stranded overhangs, or "sticky ends", are extended from the termini of the double helices to facilitate the intermolecular association of the tiles.[3] For polyvalent binding studies, the double-helical core region of the DNA tile serves as the nanoscale scaffold, with the attached sticky ends modeling the corresponding ligands/receptors of intermolecular binding. Conveniently, small variations in the design of a tile can be introduced to modify its conformational flexibility. In particular, immobile Holliday junction and double crossover tiles have demonstrated unique conformational flexibility, permitting their use as scaffolds for subsequent study.[4−15]

Holliday junction (J) tiles are composed of four DNA oligonucleotides (strands) that self-assemble into four double-helical arms, which are stacked into two helical domains connected at a single branch point, or junction.[4] The junction is formed by a reciprocal crossover, where the two linking strands traverse both helical domains at the same position (Figure 1A). There is evidence that transitions between the two possible stacking conformers occur with strong bias toward one conformer, determined by the junction sequence.[16,17] The J tiles used in the present study have been shown to adopt the stacking preference illustrated in the Supporting Information (Figure S1).[18] In addition, J tiles have been shown to have a high degree of conformational flexibility, with a wide range of angles between the arms of the junction.[19] As a result, J tiles are well suited to serve as "flexible" scaffolds.

DAE double crossover (DX) tiles consist of five single strands of DNA that self-assemble into two, side-by-side, anti-parallel helical domains with two reciprocal crossovers between the helices.[14] The distance between the intra-tile crossovers is an even number of helical half-turns, resulting in a nearly planar tile (Figure 1B). The presence of a second crossover, as compared to J tiles, restricts conformational flexibility, and DX tiles were

Received: November 17, 2010
Published: March 07, 2011

dx.doi.org/10.1021/ja1103298 | J. Am. Chem. Soc. 2011, 133, 4490–4497

found to be approximately twice as stiff as double-stranded DNA molecules of the same length.[20,21] Thus, DX tiles represent relatively "rigid" scaffolds.

Here, we report the construction of a range of dimer superstructures composed of J and DX tile monomers, which represent flexible and rigid scaffolds, respectively. For both DNA tiles, two double-helical domains in the scaffold allow construction of "bivalent molecules", with the attached sticky ends serving as the sites of intermolecular binding. The distance between the inter-tile crossover points is exactly two full turns, ensuring that both sticky ends can be paired side-by-side in the dimer. A well-established fluorescence resonance energy-transfer (FRET)-based method was employed to study the dimer assembly and disassembly reactions in real-time, permitting the determination of dimer melting temperature and calculation of thermodynamic parameters from the corresponding thermal profiles.[24,25] In this method, a FRET donor is attached to a selected strand within one DNA tile monomer, while the complementary DNA tile is labeled with the corresponding FRET acceptor. Formation of the dimer (upon cooling) brings the FRET pair into close proximity, and following the temperature-dependent change in FRET efficiency facilitates monitoring of the assembly/disassembly process.

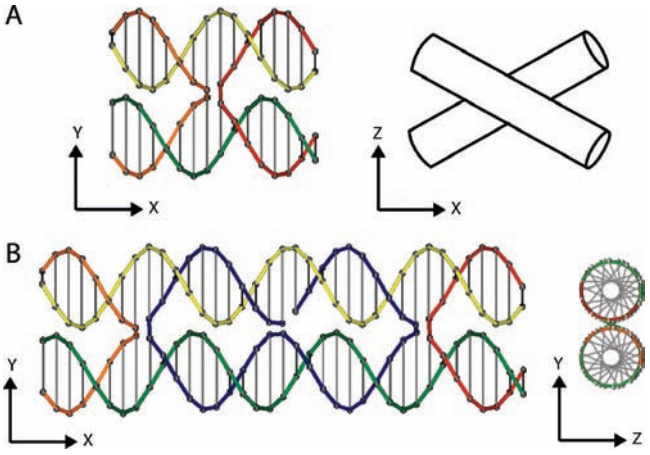

Figure 1. Helical structures of J and DX core tiles. (A) Two strands of J (yellow and green) preserve their helical structure, while the remaining two strands (red and orange) form the reciprocal crossover between the helical domains. The equilibrium distribution between the two possible crossover isomers is primarily determined by strand sequence.[16−18] J tiles are flexible at the crossover point with a variety of possible angles between arms.[11,13,22,23] Top view is shown on the right. (B) DX tiles are essentially two J tiles connected by two double-helical arms, with a cyclic central strand. The two crossover points are separated by an even number of half-turns (shown here with four half-turn separation). Side view is shown on the right.

Figure 2A−D illustrates the J and DX monomer tiles used for the assembly of dimers that can be described as flexible (J/J homo-dimer), semi-rigid (DX/J hetero-dimer), and rigid (DX/DX homo-dimer). A-type tiles (J-A and DX-A) contain two unique sticky ends that are five nucleotides each, labeled as 1 and 2, while B-type tiles (J-B and DX-B) contain sticky ends 1′ and 2′, complementary to sticky ends 1 and 2, respectively. These two pairs of complementary sticky ends link A- and B-type tiles together, creating a bivalent association between the tile scaffolds. This design, where analogous tiles share the same sticky end sequences, ensures that any observed difference in the formation of dimers from these monomeric units is a result of variations in the scaffold core (flexible vs rigid), not the nature of the ligand/receptor interaction. A yellow star and a red triangle identify the position of the FRET donor (fluorescein) and acceptor (TAMRA) fluorophores, respectively.

RESULTS AND DISCUSSION

Real-Time Monitoring of Dimer Formation. For the FRET experiments, determination of the melting temperature of dimer

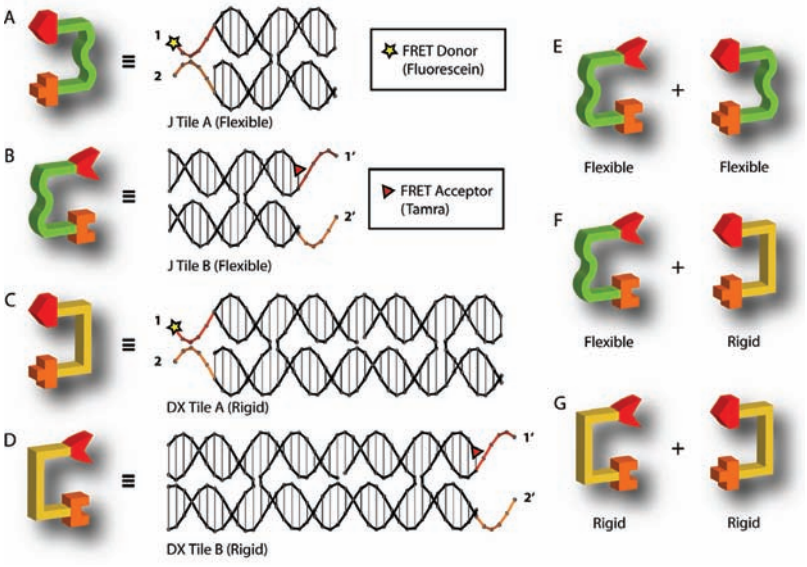

Figure 2. Schematic representation and helical structure of the J (flexible scaffold in green) and DX (rigid scaffold in yellow) tiles used in the study. FRET donor and acceptor fluorophores are shown as yellow stars (fluorescein) and red triangles (TAMRA), respectively. Two pairs of complementary sticky ends, 1/1′ and 2/2′ (shown as complementary shapes in the schematics), were added to the ends of the tiles to create a bivalent association between the scaffolds. (A) J-A (32 bp); (B) J-B (36 bp); (C) DX-A (74 bp); (D) DX-B (82 bp). The numbers mark the size of the hybridized domains in the tiles. For all dimers, the inter-tile junctions are separated by two full turns to ensure an in-plane dimer conformation. (E−G) The flexible, semi-rigid, and rigid dimers that contain J-A/J-B, J-A/DX-B, and DX-A/DX-B, respectively.

dx.doi.org/10.1021/ja1103298 |J. Am. Chem. Soc. 2011, 133, 4490–4497

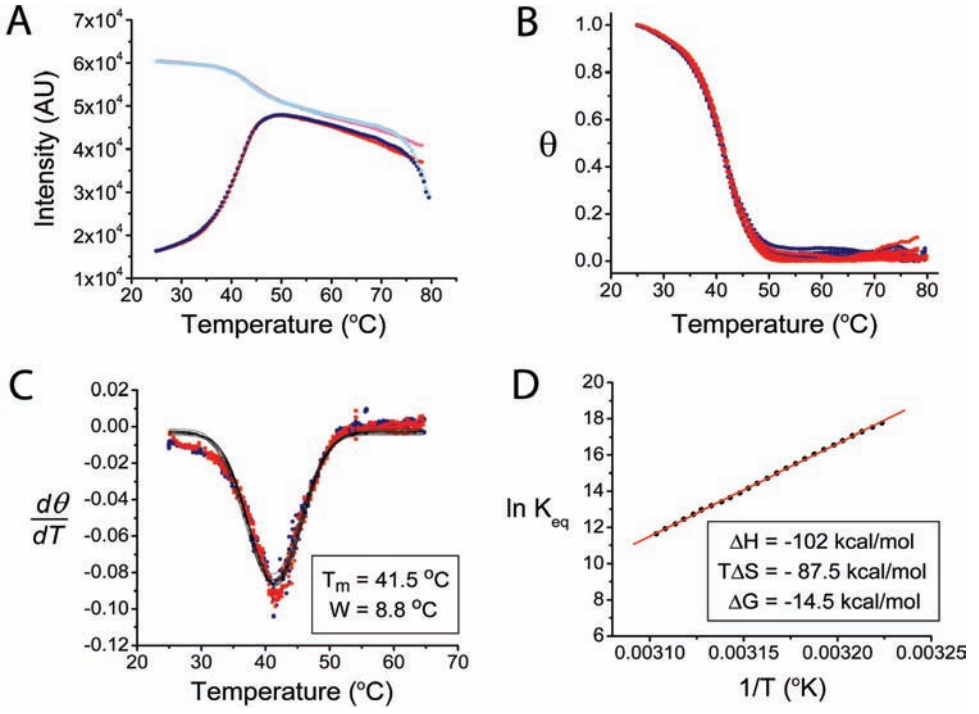

Figure 3. Illustration of FRET data analysis for a typical sample (DX-A/DX-B homo-dimer). (A) The raw data (fluorescence intensity versus temperature) were collected by a RT-PCR thermocycler. The heating and cooling curves for the donor/acceptor sample are shown in red and blue, respectively, and the heating and cooling curves for the donor-only sample are shown in magenta and cyan, respectively. (B) Plot of normalized FRET efficiency or fraction of dimer formation, θ, as a function of temperature. Multiple thermal profiles (heating cycles shown in red and cooling cycles shown in blue) are plotted together (six replicate profiles), exhibiting the negligible hysteresis and high reproducibility of the data. A single thermal transition at ~41.5 °C is observed. (C) First derivatives of the profiles in panel B, $d\theta/dT$, are plotted versus temperature (dots), and a Gaussian fit (solid line) yields the melting temperature (41.5 °C) and the width of the transition (8.8 °C). (D) The linear fit of a corresponding van't Hoff plot generates the changes of enthalpy (ΔH) and entropy ($T\Delta S$), and thereby the free energy change (ΔG).

complexes and extraction of thermodynamic parameters from thermal profiles has been previously detailed.[2,24,25] For each dimer assembly, two samples were prepared with identical experimental conditions: one sample contained a donor fluorophore (5′-fluorescein-labeled oligomer) in tile A and an acceptor fluorophore (5′-TAMRA-labeled oligomer) in tile B, while the second sample contained only the donor fluorophore in tile A and the corresponding unlabeled oligomer in tile B. Comparing the donor emission of these two samples yields the efficiency of energy transfer between the donor and acceptor. The inter-fluorophore distance (and therefore the FRET efficiency) changes as a result of temperature-dependent conformational changes, which directly reflects the assembly/disassembly process of the DNA tile dimers (the donor and acceptor pair has a Förster distance 4.8−5.0 nm). The fluorescence thermal curves were measured with a real-time PCR thermocycler: for cooling profiles, the samples were held at a high temperature (80 °C), and the fluorescent emission of the donor at 522 nm (excited at 492 nm) was monitored while the temperature was decreased to 25 °C, with a gradient of −0.1 °C/min. Heating profiles were similarly collected, and all experiments were repeated at least twice in triplicate to ensure reproducibility (see the Supporting Information (SI) for experimental details).

A comprehensive description of FRET data processing can be found in the Supporting Information. Briefly, for each dimer assembly: (1) The efficiency of energy transfer (E) is determined at each temperature on the basis of the intensity of donor/acceptor (I_{DA}) and donor-only (I_D) samples (typical results shown in Figure 3A, SI eq 1). (2) E is subsequently related to the fraction of assembled dimer structures (θ) by normalizing the FRET efficiencies as a function of temperature (SI eq 2). θ is plotted against temperature with heating and cooling profiles superimposed (Figure 3B). It is important to note that negligible hysteresis was observed for all dimer assemblies, especially for the normalized data, indicating the reversibility of the dimer formation and dissociation processes and thermal equilibrium at each temperature. (3) The melting temperature (T_m) is obtained by fitting the first derivative of θ versus temperature with a Gaussian function and identifying the midpoint of the transition (Figure 3C, SI eq 3). (4) As each of the dimer assemblies demonstrated a reversible thermal transition, it can be assumed that the system reached equilibrium at each temperature, allowing application of the van't Hoff law where the variation of the equilibrium constant (K_{eq}) with temperature is used to obtain the enthalpy (ΔH) and entropy changes (ΔS) of the complex formation. K_{eq} of dimer formation is expressed as a function of θ at equilibrium, based on a bi-molecular reaction scheme (SI eq 4). Plots of $\ln K_{eq}$ vs $1/T$ in the temperature range of the transitions were linear, indicating that ΔH and ΔS are temperature independent (Figure 3D, SI eq 5). (5) Finally, the van't Hoff enthalpy and entropy changes for the reversible thermal transitions allow the calculation of the free energy change (ΔG) for the assembly process using the Gibbs equation (SI eq 6).

The results of the FRET data analysis for each of the dimer designs illustrated in Figure 2E−G are listed in Table 1.

Examination of the experimental results reveals that subtle changes in the conformational flexibility of the bivalent

dx.doi.org/10.1021/ja1103298 |J. Am. Chem. Soc. 2011, 133, 4490–4497

Table 1. Melting Temperature and Thermodynamic Characterization of Dimers Composed of Bivalent Monomer Scaffolds (J and DX) with Variable Conformational Flexibility[a]

	T_m (°C)	$W/2$ (°C)	ΔH (kcal/mol)	ΔS (kcal/mol·K)	$T\Delta S$ (kcal/mol)	ΔG (kcal/mol)
flexible dimer	31.0 ± 0.6	4.3	−123.2 ± 9.1	−0.373 + 0.030	−113.3 ± 9.1	−11.9 ± 0.1
semi-rigid dimer	36.2 ± 0.6	4.8	−106.8 ± 3.9	−0.314 ± 0.012	−93.5 ± 3.7	−13.3 ± 0.2
rigid dimer	41.4 ± 0.2	4.3	−102.0 ± 1.4	−0.293 ± 0.004	−87.5 ± 1.3	−14.5 ± 0.1

[a] The structures of the monomer units are shown in Figure 2. The values listed are the mean and standard deviation of measurements from multiple thermal profiles (six independent samples, with analysis of the heating and cooling cycle for each). $W/2$ indicates the half-width of the Gaussian fit, representing the width of the thermal transition (Figure 3C). The temperature used to calculate $T\Delta S$ and ΔG is 25 °C. The concentration of the individual tiles in each sample is 0.3 μM. The details of data analysis are described in the Supporting Information.

monomer scaffolds lead to significant differences in the thermal stability of the dimer superstructures. The melting temperature was the highest, ~41 °C, for dimers composed of two rigid scaffolds (DX/DX homo-dimer) and the lowest, ~31 °C, when both scaffolds were flexible (J/J homo-dimer). The 10 °C difference in the melting temperatures of these two DNA tile dimers is rather remarkable considering that both dimer structures have identical sticky end sequences. The semi-rigid (J/DX hetero-dimer) construct had a melting temperature of ~36 °C, the mid-point between the flexible and rigid dimers.

The change in free energy reflected the same trend: the rigid dimer requires the smallest conformational change of each monomer unit, and thus it shows the most favorable binding, with the most negative ΔG. Interestingly, introducing flexibility into the scaffold significantly affects the changes in both the enthalpy and entropy of the corresponding dimerization reaction. For example, comparing the semi-rigid and rigid dimers, ΔG for the semi-rigid dimer formation is ~1.2 kcal/mol less negative than that of the rigid dimer, which can be translated to an ~10-fold reduction of the equilibrium constant at room temperature. This difference in ΔG is mostly the result of a more negative $T\Delta S$, originating from the larger entropic cost to form a J/DX tile compared to a rigid DX/DX dimer. On the other hand, for a flexible J/J dimer, its formation significantly restricts the range of branch angles that are available to the J monomers and carries a corresponding entropic penalty. It should be noted that both the ΔH and $T\Delta S$ values for the flexible dimer are significantly more negative than those for the rigid dimer (with $T\Delta S$ exhibiting a larger difference). This result indicates that the association of two flexible tiles involves a more favorable enthalpic gain. This may be because the junction flexibility permits enhanced hydrogen-bonding interactions and more favorable base stacking between the sticky ends and their flanking base pairs, thus resulting in reduced energetic strain within the helical arms in the final dimer assembly. However, this enthalpic gain is completely offset by an even greater entropic loss because the conformations available to both monomeric units are largely restricted upon dimer formation. Overall, the thermodynamic effects result in a flexible dimer that is less thermally stable than the corresponding rigid dimer.

Competitive Displacement Reactions. The relative stability of the dimers was further demonstrated through competition assays, and the results were visualized using polyacrylamide gel electrophoresis (PAGE) (see the SI for experimental details). Figure 4 illustrates the three competitive displacement reactions that were performed, each involving the addition of an increasing amount of secondary tile to a pre-assembled dimer.

Three possible outcomes of the displacement reactions are predicted on the basis of the relative thermal stability of the corresponding dimers: complete, partial, or no exchange of one tile in the initial dimer by the secondary tile. For the case in which the initial dimer is relatively less stable than the replacement dimer, as applies to the schemes shown in Figure 4A and B, quantitative displacement should be observed. For the case in which the initial dimer is relatively more stable, as shown in Figure 4C, minimal formation of the replacement dimers would be detected, even with a large excess of the secondary tile present.

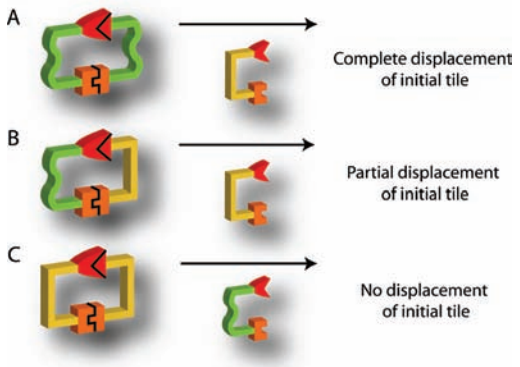

Figure 4. Schematic representation of the competitive displacement reactions. Each tile of the initial dimer is present at equimolar concentration and labeled with a fluorescent dye. The unlabeled secondary tiles are added in a range of relative concentrations, from submolar to excess compared to the initial tiles. (A) Rigid DX tile is added to pre-assembled flexible J/J dimer. (B) Rigid DX tile is added to pre-assembled semi-rigid J/DX tile. (C) Flexible J tile is added to pre-assembled rigid DX/DX dimer.

To make identification of the gel bands corresponding to each individual tile and the assembled dimers possible, the tiles in the initial dimers were labeled with two fluorescent dyes, fluorescein and TAMRA. The dyes were placed at positions away from the intermolecular, sticky-end binding sites (different from those used in the FRET experiment with inter-dye distances a minimum 10 nm in the dimer) to minimize energy transfer between the fluorophores, so that the intensities of the fluorescent bands measured from the gel images provide a semi-quantitative measure of the concentration of the species they represent (see SI for details). In addition, the tiles (secondary) that were added to the pre-assembled dimers contained no dye label, so that both a color change and a gel shift are expected if any exchange reaction occurs. Multicolor gel images were generated by superimposing the fluorescent intensity of the green (fluorescein) and red (TAMRA) channels (collected with a Typhoon Trio gel imaging system).

The results of the competitive displacement experiments are in agreement with the predictions based on the FRET study. Figure 5 shows typical PAGE results for the reactions represented in Figure 4 (additional gel images are shown in the SI Figures 3−18).

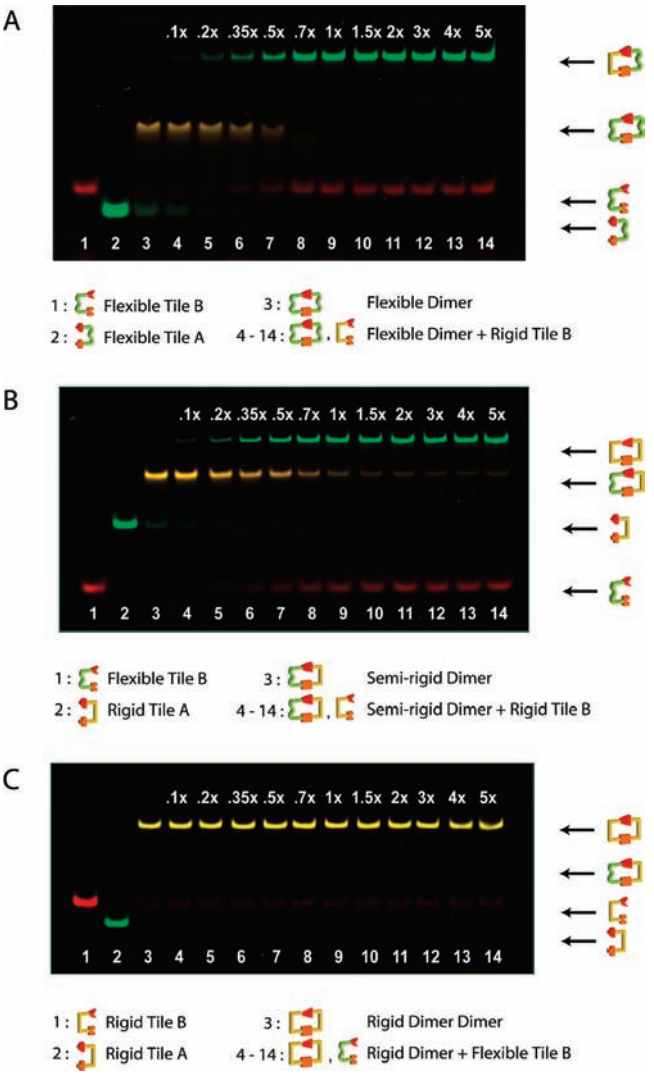

Figure 5. Polyacrylamide gel analysis of the reaction schemes shown in Figure 4, at 20 °C. The gel images represent overlay of both green and red fluorescent channels. (A) Rigid DX tile added to pre-assembled flexible J/J dimer. (B) Rigid DX tile added to pre-assembled semi-rigid J/DX tile. (C) Flexible J tile added to pre-assembled rigid DX/DX dimer. Lanes 4−14 represent an increasing amount of secondary tile, with the molar ratio to the initial dimer ranging from 0.1:1 to 5:1. The amount of secondary tile (compared to 1× initial dimer) is indicated above the top band in each gel. The displacement reactions for all three cases were allowed to proceed for 2 h before loading onto the gel for analysis. Additional gels for each reaction at various temperatures and different reaction times are included in the Supporting Information.

For each gel, lanes 1−3 contain the individual monomer units and their pre-formed 1:1 dimers, respectively. In addition to confirming the formation of each individual tile and the initial dimer, these bands (which have a unique size and fluorescent label) also serve as markers that help to determine the identity of each band in the remaining lanes. Lanes 4−14 correspond to the displacement reactions that contain the initial dimer with increasing amounts of secondary tile (see the SI for experimental details). The presence and relative concentrations of all species in the gels before and after the replacement reaction can be determined by measuring the fluorescent intensity of the corresponding bands.

The gel image in Figure 5A shows the equilibrium shift when the pre-formed J-A/J-B homo-dimer was mixed with increasing amounts of DX-B secondary tile. The displacement of J-B in the initial dimer by DX-B to form a J-A/DX-B hetero-dimer is readily observed, as evidenced by the disappearance of the middle yellow J-A/J-B dimer band, the simultaneous appearance of a lower red band (displaced J-B), and the appearance of an upper green band (the newly formed J-A/DX-B dimer). Note that the secondary DX-B tile is unlabeled, and the newly formed dimer contains only the green fluorescent label on J-A. The pattern of intensity changes that occur for each of the various bands supports the prediction of a quantitative displacement reaction, confirming that the semi-rigid J/DX dimer is thermodynamically more favored than the flexible J/J dimer.

Similarly, the PAGE result shown in Figure 5B that corresponds to the reaction of pre-assembled J-B/DX-A dimer with DX-B as the secondary tile revealed that the favored reaction product is the rigid DX/DX dimer, with quantitative displacement of J-B in the dimer by DX-B. However, the PAGE result in Figure 5C, corresponding to the reaction of initial DX/DX dimer with J-B as the secondary tile, showed that the dominant species in each reaction mixture was the initial, rigid DX/DX dimer, with little or no replacement of DX-B by J-B detected, even with a 5× molar excess of the secondary J tile. Collectively, the PAGE experiments support the conclusions drawn from the FRET experiments: dimers composed of two rigid tiles are more stable than those composed of one rigid and one flexible tile, and dimers composed of two flexible tiles are the least favored.

For each dimer, the entropy change of formation has a fairly large negative value (see Table 1), so it is expected that the relative equilibrium of the dimers will change with temperature. For example, compared to the J/DX dimer, formation of the J/J dimer involves a more negative entropy change, implying that the J/J dimer should exhibit a greater increase in equilibrium binding constant at lower temperatures. The ratio of the J/DX dimer equilibrium constant to that of the J/J dimer (as calculated from the ΔG values) is ~1 at 5 °C, compared to ~5 at 20 °C. Indeed, gel results (SI Figures 3−14) reflect the temperature dependence of the equilibrium constants: for displacement reactions carried out at temperatures ranging from 5 to 20 °C, only partial exchange was observed at lower temperatures. At 5 °C, ~30% of the initial J/J dimer (yellow band) remained, even with an excess of DX secondary tile compared to the J/J dimer, in contrast to the 20 °C reaction, in which this band completely disappeared. The same trend was observed for the J/DX displacement reaction (DX secondary tile), in which the ratio of the DX/DX dimer equilibrium constant to that of J/DX dimer is expected to change from ~10 at 20 °C to ~6 at 5 °C. Collectively, the results of the gel assays for all three displacement reactions are in agreement with the thermodynamic data obtained by the FRET experiments.

Tiles with Variable Flexibility. To further study how the flexibility of a bivalent scaffold affects its association, two additional series of modified J tiles (in which the flexibility of the tiles were finely tuned) were constructed. The modified tiles were designed to form homo-dimers, and FRET analyses revealed an intriguing detail: the enthalpy and entropy changes associated with dimerization have partly compensating effects on strength of binding. In addition, the thermodynamics of polyvalent dimer formation clearly reflects the flexibility of the monomeric components.

The first series of modified J tiles, referred to as mesojunction tiles (Figure 6A), are similar to J tiles but have two individual

dx.doi.org/10.1021/ja1103298 |J. Am. Chem. Soc. 2011, 133, 4490–4497

crossovers at separate positions between the two helical domains rather than a single reciprocal crossover, and this structural feature is expected to result in an overall increase in the conformational flexibility of the scaffold.[26,27] Only A-type tiles (with sticky ends 1 and 2) are shown in Figure 6. The complementary B-type tiles (with sticky ends 1′ and 2′) have the same design (SI Figure 1). One of the strands that connect the two helical domains contains a variable number of thymine nucleotides (2T, 4T, or 6T), forming a single-stranded loop (shown in blue in Figure 6A) on the opposite side as the sticky ends (shown in red/orange). Among this series, the structure of the 2T mesojunction tile is expected to be the most constrained, while the 6T mesojunction tile should be the most flexible.

As shown in Table 2, all three mesojunction tile dimers have nearly the same melting temperature (T_m) and free energy change (ΔG), with values of ~30 °C and −12 kcal/mol, respectively, which are very similar to those of the flexible J/J dimer.

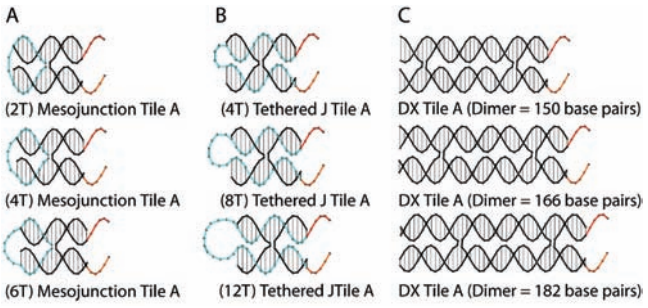

Figure 6. Helical structure of modified J tiles of varying flexibility and DX tiles of various size. (A) Series of mesojunction tiles. To further tune the flexibility, the arms of the tile were constrained by varying the number of thymines (T) within one of the crossover strands (shown in blue), forming a single-stranded loop of 2, 4, or 6T's. Note that the helical domains are not connected by a reciprocal crossover, as in a J tile, but are connected by two separate single-stranded crossovers. The blue strand has a nick at the junction position. (B) Series of tethered J tiles. For this series, the helical domains of each tile are connected by a reciprocal crossover, the same as in the unmodified J tiles. To reduce the flexibility of the scaffold, the two strands of the tile that do not participate in the crossover are connected by a short loop of 4, 8, or 12 T's, respectively, shown in blue. (C) Series of DX-A tiles of various sizes: 70, 78, and 86 bp, respectively. Binding of the DX-A tiles to their corresponding DX-B tiles results in 150, 166, and 182 bp homodimers.

These results suggest that the mesojunction dimers have a thermal stability comparable to that of the J/J dimers, and the addition of multiple T's within each mesojunction tiles does not significantly affect their formation or participation in a dimer superstructure. However, the decrease in tile flexibility as the number of T's is reduced results in considerable differences in the enthalpy (ΔH) and entropy (ΔS) changes associated with dimer formation. The ΔH values for mesojunction dimer formation exhibit a clear trend (2T > 4T > 6T), becoming more negative as the loop size is increased; ΔS follows the same pattern. Meanwhile, all the mesojunction dimers have comparable ΔG of formation. This indicates that, while increasing the conformational flexibility of the participating scaffolds (with longer T loop) increases the entropic cost of dimer association, the same flexibility results in a more favorable gain in enthalpy, and these two effects are compensating, resulting in a similar thermal stability for all of the mesojunction dimers at room temperature. Compared to the unmodified, flexible J/J dimer, the ΔH values for mesojunction dimers are significantly more negative (more favorable), and the ΔS values are also more negative (less favorable). The mesojunction tiles are the only series of tiles that do not have a reciprocal crossover at the junction, resulting in a significant increase in the freedom of motion around the junction point. This freedom may interfere with the base stacking of nucleotides flanking the junction in unbound tiles. Dimerization of the mesojunction tiles will constrain the junction and improve the base stacking for both tiles involved, thus resulting in a much more favorable change in enthalpy upon binding as compared to the other tile dimers. An approximate calculation indicates that 2−4 additional base-stacking interactions can account for the more negative ΔH for mesojunction dimer formation than for the J/J dimer.

The second series of the modified J tiles are referred to as tethered J tiles (Figure 6B), and like J tiles, they consist of four strands of DNA with a reciprocal crossover between the double-helical domains. However, the two strands that do not participate in the crossover are linked by a short loop of thymines (shown in blue in Figure 6B), ranging from 4T to 12T. Compared to unmodified J tiles, the entire series of tethered J tiles should be more constrained, with the tethered loop preventing free movement about the junction point.

The results of the FRET experiments reveal that the thermal stabilities of homo-dimers formed from the tethered tile series

Table 2. Melting Temperature and Thermodynamic Characterization of Dimers Composed of Bivalent Monomer Scaffolds (Modified J and DX) with Variable Conformational Flexibility and Size[a]

	T_m (°C)	$W/2$ (°C)	ΔH (kcal/mol)	ΔS (kcal/mol·K)	$T\Delta S$ (kcal/mol)	ΔG (kcal/mol)
2T mesojunction dimer	29.1 ± 0.3	2.8	−140.5 ± 6.6	−0.433 ± 0.022	−129.2 ± 6.5	−11.3 ± 0.1
4T mesojunction dimer	30.6 ± 0.5	2.6	−169.2 ± 5.6	−0.526 ± 0.019	−156.8 ± 5.6	−12.4 ± 0.3
6T mesojunction dimer	30.7 ± 0.2	2.6	−180.4 ± 9.7	−0.563 ± 0.032	−167.8 ± 9.6	−12.6 ± 0.2
4T tethered J dimer	35.4 ± 0.2	4.5	−108.2 ± 1.8	−0.320 + 0.006	−95.3 ± 1.7	−12.9 ± 0.1
8T tethered J dimer	36.0 ± 0.8	4.4	−105.1 ± 3.0	−0.309 ± 0.010	−92.1 ± 2.9	−13.0 ± 0.2
12T tethered J dimer	34.3 ± 0.4	4.4	−103.0 ± 2.9	−0.303 ± 0.010	−90.4 ± 2.8	−12.6 ± 0.2
rigid dimer (182 bp)	41.4 ± 0.3	4.5	−99.7 ± 1.2	−0.286 ± 0.004	−85.3 ± 1.2	−14.4 ± 0.1
rigid dimer (166 bp)	41.4 ± 0.2	4.3	−102.0 ± 1.4	−0.293 ± 0.004	−87.5 ± 1.3	−14.5 ± 0.1
rigid dimer (150 bp)	41.5 ± 0.1	4.1	−104.2 ± 0.4	−0.300 ± 0.001	−89.6 ± 0.3	−14.6 ± 0.1

[a] The structures of the monomer units are shown in Figure 6. The values listed are the mean and standard deviation of measurements from multiple thermal profiles (three independent samples, with analysis of the heating and cooling cycle for each). $W/2$ indicates the half-width of the Gaussian fit, representing the width of the thermal transition (Figure 3C). The temperature used to calculate $T\Delta S$ and ΔG is 25 °C. The concentration of the individual tiles in each sample is 0.3 μM. The details of data analysis are described in the Supporting Information.

dx.doi.org/10.1021/ja1103298 |J. Am. Chem. Soc. 2011, 133, 4490–4497

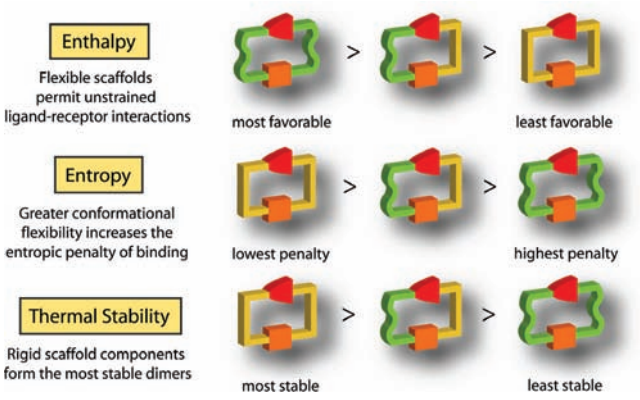

Figure 7. Result summary: the conformational flexibility of two scaffolds linked by bivalent associations affects the enthalpy, entropy, and thermal stability of their binding.

are similar to that of the semi-rigid J/DX hetero-dimer, with melting temperatures of ~35, 36, and 34 °C for 4T, 8T, and 12T tiles, respectively. The ΔG values for this series of tiles also mirror that of the J/DX hetero-dimer, ~ −13 kcal/mol. Interestingly, varying the number of T's that connect the two helical arms of the tiles does not result in significant differences in ΔH and ΔS. The range of ΔH, from ~ −108 kcal/mol for the 4T tile dimer to ~ −103 kcal/mol for the 12T tile dimer, is about the same as for the semi-rigid hetero-dimer (~ −107 kcal/mol). Similarly, $T\Delta S$ varies from ~ −95 kcal/mol for the 4T tile dimer to ~ −90 kcal/mol for the 12T tile dimer, also about the same range as fpr the J/DX hetero-dimer (~ −94 kcal/mol). Overall, the entire series of tethered J tiles behave as relatively rigid scaffolds, and it seems that increasing the number of T's in the tether loop from 4 to 12 does not effectively relieve the constraint.

Finally, to determine if variations in size (not only flexibility) would impact the binding affinities of the DNA tile scaffolds, several sizes of DX/DX dimers (150, 166, and 182 bp) were evaluated (Figure 6C). The experimental data (Table 2) suggest that the size of the scaffold has very little effect on the thermal stability of the resulting dimers, as the melting temperature and ΔG values for all three DX/DX dimers were approximately equal. The ΔH and $T\Delta S$ values of the smallest and largest dimers varied by less than 5 kcal/mol (demonstrating a small but notable dependence on size), again compensating for each other and yielding similar ΔG values. The sole difference in the three tiles is on the side opposite the sticky ends (the DNA strand sequence and length of all common regions are identical). One possible explanation for the observed difference in ΔH and ΔS is that stabilization in the central, sticky-end region of the dimer may propagate throughout the complex, further improving base stacking in the periphery. It seems that the more extended (larger) the tile is, the less susceptible it is to long-range stabilization. However, size-dependent effects cannot account for the ΔH and ΔS differences observed in the other experiments. The results suggest that the variation in the thermal stabilities of the other dimer assemblies is the product of differences in the conformational flexibility of the DNA scaffolds, and not merely a consequence of component tile size.

CONCLUSIONS

It is generally accepted that the flexibility of a DNA nanoscaffold is related to the number of connections between helical domains, with the least rigid structures formed from the fewest number of crossovers. Besides the number of crossovers, the structure of the connection points influences the overall flexibility of the tile; e.g., compared to single crossovers, reciprocal crossovers are more rigid. It is also evident that appropriate use of thymine tethers can restrict the motion of the junction points, thereby reducing the conformational flexibility of the tiles. With these design parameters in mind, a collection of DNA tiles were constructed to characterize the influence of conformational flexibility on multivalent scaffold binding.

The most significant insights gained by this multivalent binding study are illustrated in Figure 7. First, increasing the conformational flexibility of a bivalent scaffold increases the entropic cost of association; however, the same flexibility results in a more favorable enthalpy of binding. This can be understood in the following way: imposing order on a flexible object through a binding event will carry an entropic penalty; on the other hand, adequate flexibility increases the likelihood that all ligand−receptor interactions can occur without energetic strain. Second, the overall thermal stability of bivalently linked scaffolds is highest when both scaffold components are rigid and lowest when both scaffolds are flexible. This observation indicates that reducing the entropic cost of association plays an important role in increasing the overall thermal stability.

This study demonstrates how precisely engineered DNA nanostructures can be used to probe very subtle biophysical phenomena, including the effect of scaffold flexibility on the binding of a multivalent molecule. The use of DNA nanostructures as models of polyvalent binding has made it possible to quantify the compensating effects of enthalpy and entropy, which is a notoriously difficult relationship to characterize. This technique may be used to generate valuable structural and functional characterizations and may have applications in various research fields, such as polyvalent inhibitor drug discovery and the study of spatially controlled chemical reactions.

ASSOCIATED CONTENT

Supporting Information. Experimental details, description of FRET data processing and results, tile design and DNA sequences, and additional PAGE results. This material is available free of charge via the Internet at http://pubs.acs.org.

AUTHOR INFORMATION

Corresponding Author
yan_liu@asu.edu

ACKNOWLEDGMENT

This research was partly supported by grants from the Army Research Office, Office of Naval Research, National Science Foundation, Department of Energy, and National Institutes of Health to Y.L. and from the Army Research Office, Office of Naval Research, National Science Foundation, Department of Energy, National Institutes of Health, and Sloan Research Foundation to H.Y. Y.L. and H.Y. were supported by the Technology and Research Initiative Fund from Arizona State University and as part of the Center for Bio-Inspired Solar Fuel Production, an Energy Frontier Research Center funded by the U.S. Department of Energy, Office of Science, Office of Basic Energy Sciences under Award Number DE-SC0001016.

REFERENCES

(1) Mammen, M.; Choi, S. K.; Whitesides, G. M. *Angew. Chem. Int. Ed.* **1998**, *37*, 2754–2794.
(2) Nangreave, J.; Yan, H.; Liu, Y. *Biophys. J.* **2009**, *97*, 563–571.
(3) Seeman, N. C. *J. Theor. Biol.* **1982**, *99*, 237–247.
(4) Seeman, N. C.; Kallenbach, N. R. *Biophys. J.* **1983**, *44*, 201–209.
(5) Kallenbach, N. R.; Ma, R. I.; Seeman, N. C. *Nature* **1983**, *305*, 829–831.
(6) Marky, L. A.; Kallenbach, N. R.; McDonough, K. A.; Seeman, N. C.; Breslauer, K. J. *Biopolymers* **1987**, *26*, 1621–1634.
(7) Cooper, J. P.; Hagerman, P. J. *J. Mol. Biol.* **1987**, *198*, 711–719.
(8) Churchill, M. E. A.; Tullius, T. D.; Kallenbach, N. R.; Seeman, N. C. *Proc. Natl. Acad. Sci. U.S.A.* **1988**, *85*, 4653–4656.
(9) Duckett, D. R.; Murchie, A. I. H.; Diekmann, S.; von Kitzing, E.; Kemper, B.; Lilley, D. M. J. *Cell* **1988**, *55*, 79–89.
(10) Cooper, J. P.; Hagerman, P. J. *Proc. Natl. Acad. Sci. U.S.A.* **1989**, *86*, 7336–7340.
(11) Murchie, A. I. H.; Clegg, R. M.; von Kitzing, E.; Duckett, D. R.; Diekmann, S.; Lilley, D. M. J. *Nature* **1989**, *341*, 763–766.
(12) Lu, M.; Guo, Q.; Marky, L. A.; Seeman, N. C.; Kallenbach, N. R. *J. Mol. Biol.* **1992**, *223*, 781–789.
(13) Mao, C.; Sun, W.; Seeman, N. C. *J. Am. Chem. Soc.* **1999**, *121*, 5437–5443.
(14) Fu, T. J.; Seeman, N. C. *Biochemistry* **1993**, *32*, 3211–3220.
(15) Winfree, E.; Liu, F.; Wenzler, L. A.; Seeman, N. C. *Nature* **1998**, *394*, 539–544.
(16) Miick, S. M.; Fee, R. S.; Millar, D. P.; Chazin, W. J. *Proc. Natl. Acad. Sci. U.S.A.* **1997**, *94*, 9080–9084.
(17) McKinney, S. A.; Declais, A.-C.; Lilley, D. M. J.; Ha, T. *Nat. Struct. Biol.* **2002**, *10*, 93–97.
(18) Altona, C. *J. Mol. Biol.* **1996**, *263*, 568–581.
(19) Petrillo, M. L.; Newton, C. J.; Cunningham, R. P. *Biopolymers* **1988**, *27*, 1337–1352.
(20) Li, X.; Yang, X.; Qi, J.; Seeman, N. C. *J. Am. Chem. Soc.* **1996**, *118*, 6131–6140.
(21) Sa-Ardyen, P.; Vologodskii, A. V.; Seeman, N. C. *Biophys. J.* **2003**, *84*, 3829–3837.
(22) von Kitzing, E.; Lilley, D. M. J.; Diekmann, S. *Nucleic Acids Res.* **1990**, *18*, 2671–2683.
(23) Eis, P. S.; Millar, D. P. *Biochemistry* **1993**, *32*, 13852–13860.
(24) Sacca, B.; Meyer, R.; Feldkamp, U.; Schroeder, H.; Niemeyer, C. M. *Angew. Chem. Int. Ed.* **2008**, *47*, 2135–2137.
(25) Sacca, B.; Meyer, R.; Niemeyer, C. M. *Nat. Protoc.* **2009**, *4*, 271–285.
(26) Du, S. M.; Zhang, S.; Seeman, N. C. *Biochemistry* **1991**, *31*, 10955–10963.
(27) Wang, H.; Seeman, N. C. *Biochemistry* **1995**, *34*, 920–929.